New Type of Bonding Formed from an Overlap between π Aromatic and π^* C═O Molecular Orbitals Stabilizes the Coexistence in One Molecule of the Ionic and Neutral meso-Ionic Forms of Imidazopyridine

Marcin Hoffmann,*,†,§ Agnieszka Plutecka,† Urszula Rychlewska,*,† Zdzislaw Kucybala,‡ Jerzy Paczkowski,‡ and Ilona Pyszka‡

Faculty of Chemistry, Adam Mickiewicz University, Grunwaldzka 6, 60-780 Poznan, Poland, Faculty of Chemical Technology and Engineering, University of Technology and Agriculture, Seminaryjna 3, 85-236 Bydgoszcz, Poland, and BioInfoBank Institute, Limanowskiego 24 A, 60744 Poznan, Poland

Received: November 15, 2004; In Final Form: March 9, 2005

New bis(imidazo)pyridine dye has been synthesized and tested as a potential photoinitaitor for free-radical polymerization induced with the visible emission of an argon ion laser. The X-ray analysis based on data collected at 170 and 130 K, as well as density functional theory (DFT) calculations, revealed the presence of two different forms of imidazopyridine rings within the same molecule. These two forms of the same moiety had not only different geometries but different electronic structures as well. One of the imidazopyridine rings was in the ionic form, while the other was in the meso-ionic form. DFT calculations provided an explanation for such an observed phenomena. The averaging of ionic and meso-ionic forms of imidazopyridine rings within the same molecule is hindered because of an attractive interaction between them. Analysis of electronic density revealed that, indeed, a new type of bonding is formed as the result of an overlap between π aromatic and π^* C═O molecular orbitals. This bonding, like the hydrogen bond, is primarily of electrostatic character, and its energy was estimated at 3.5 kcal/mol.

Introduction

It has been reported[1,2] that the 2-oxo-2,3-dihydro-1*H*-imidazo-[1,2-a]pyridinium compounds can exist in ionic and meso-ionic forms (See Scheme 1).

We have recently synthesized a new compound that contains both of these forms in one molecule (See Scheme 2). The molecular structure of this compound has been confirmed by X-ray crystallography. To solve an intriguing question about the factors that govern the coexistence in one molecule of two different electronic forms of the same functional group, we have performed a series of DFT calculations. Presented in this paper are the synthetic route that leads to the formation of this new compound, the confirmation of its structure by X-ray diffraction methods, and DFT calculations which indicate the existence of a new type of chemical bonding formed from an overlap between the π aromatic and π^* C═O molecular orbitals.

Experimental Section

Substrates used for the preparation of the dye were purchased from Aldrich and were used without further purification. 2-Oxo-2,3-dihydro-1*H*-imidazo[1,2-a]pyridinium (IMP) bromide was prepared using methods described elsewhere[3]. Its structure, after purification with the use of preparative thin-layer chromatography, was confirmed by ^{1}H NMR and ^{13}C NMR spectroscopy.

Synthesis. Preparation of 3-[(2-oxoimidazo[1,2-a]pyridin-3-yl)pyridin-4-ylmethylene]-2-oxo-2,3-dihydro-1*H*-imidazo[1,2-a]pyridinium bromide (MII). 4-Pyridine carboxaldehyde (PCA) (0.563 g, 5.26 mmol) was dissolved under magnetic stirring in 20 mL of methanol at room temperature. To the solution, 1.132 g (5.26 mmol) of 2-oxo-2,3-dihydro-1*H*-imidazo[1,2-a]pyridinium (IMP) bromide was added dropwise. The resulting solution turned from colorless to violet with the formation of a

SCHEME 1: Ionic and meso-Ionic Forms of Imidazopyridine Moieties.

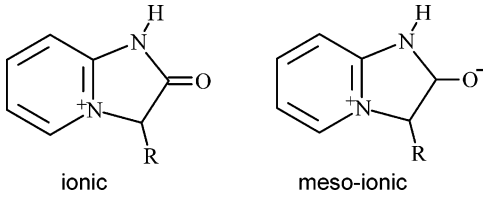

SCHEME 2: Chemical Diagram of 2-Oxo-2,3-dihydro-1*H*-imidazo[1,2-a]pyridine with the Ionic and meso-Ionic Imidazopyridine Moieties.

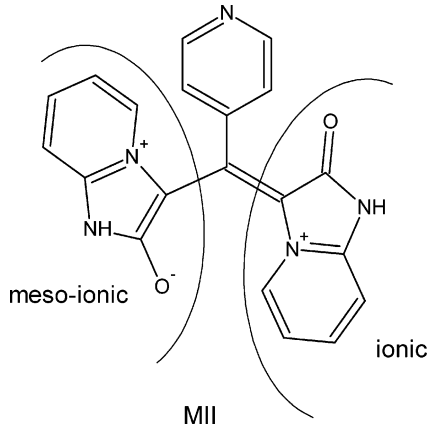

* E-mail addresses: hoffmann@man.poznan.pl (M.H.); urszular@amu.edu.pl (U.R.).
† Adam Mickiewicz University.
‡ University of Technology and Agriculture.
§ BioInfoBank Institute.

10.1021/jp0447892 CCC: $30.25
Published on Web 04/28/2005

SCHEME 3: Proposed Mechanistic Pathway of 3-[(2-Oxoimidazo[1,2-a]pyridin-3-yl)pyridin-4-ylmethylene]-2-oxo-2,3-dihydro-1*H*-imidazo[1,2-a]pyridinium Bromide Synthesis.

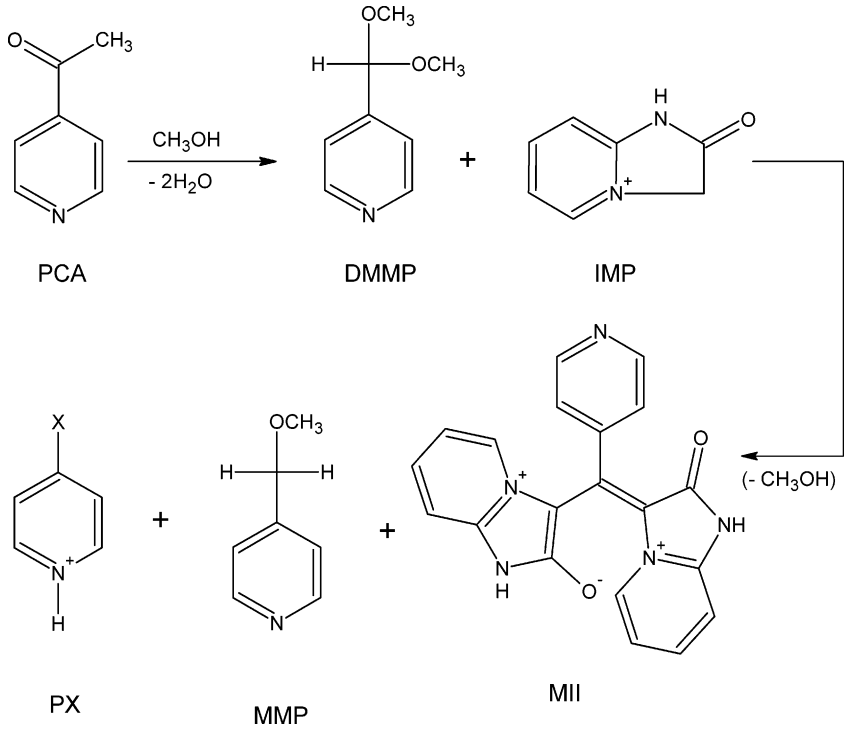

precipitate. The reaction mixture was stirred for 1 h at room temperature, yielding the final product which, after filtration, was purified by recrystallization from methanol to give dark green crystals of MII (0.59 g; yield 46.2%); mp 268−269 °C.

Mechanistic details of MII synthesis were deduced after the analysis of the structures of intermediates and products obtained during the synthesis. They were identified with the use of ^{1}H NMR spectroscopy. For the analysis, instead of methanol, CD_3OD was used as the solvent. After 2.32 mmol of PCA was dissolved in 4.64 mmol of CD_3OD, 4-dimethoxymethylpyridine (DMMP) was obtained as an intermediate: ^{1}H NMR (CD_3OD) δ 3.34 (s, 6H, OCH_3), 5.52 (s, 1H, OCHO); ^{1}H NMR ($CDCl_3$) δ 3.33 (s, 6H, OCH_3), 5.4 (s, 1H, OCHO).[4] The analysis of the final reaction mixture, apart from MII, indicated the presence of 4-methoxymethylpyridine (MMP) (^{1}H NMR (CD_3OD) δ 3.53 (s, 3H, OCH_3), 4.51 (s, 2H, CH_2); ^{1}H NMR ($CDCl_3$) δ 3.43 (s, 3H, OCH_3), 4.46 (s, 2H, CH_2))[5] and the absence of IMP or DMMP. The hydrobromide resulting from the synthesis was bound by unidentified pyridinium derivatives.

The analysis of intermediates and products allows us to propose a reasonable mechanistic pathway for the formation of 3-[(2-oxoimidazo[1,2-a]pyridin-3-yl)pyridin-4-ylmethylene]-2-oxo-2,3-dihydro-1*H*-imidazo[1,2-a]pyridinium bromide (Scheme 3).

X-ray Diffraction. Metallic green prismatic crystals were used to measure the intensity data with a KM4CCD κ-geometry diffractometer[6] equipped with graphite monochromated Mo Kα radiation (λ = 0.71073 Å) at 170 K. Following the suggestions made by one of the referees, we repeated the X-ray experiment at 130 K, but no significant changes either in the geometry of the molecule or in the crystal structure were detected. Both crystal structures have been deposited at CCDC,[7] but the results presented in this paper are based on the data obtained at 170 K. Data reduction and analysis were carried out with *CrystAlis RED*.[8] The structure was solved by direct methods using *SHELXS 86*[9,10] and refined by least-squares techniques with *SHELXL 97*.[11] The intensity data were corrected for Lp effects as well as absorption.[12] Anisotropic displacement parameters were employed for non-hydrogen atoms. The positions of the hydrogen atoms were determined from the analysis of the difference Fourier maps and refined isotropically. The relevant crystal data collection and refinement parameters are listed in Table 1.

Quantum Chemical Calculations. The structure observed in the crystals was used as a starting point for DFT full geometry optimization with the B3LYP[13,14] method (Becke's three-parameter functional with the Lee−Yang−Parr exchange-correlation potential[15]) at the split-valence double-ζ 6-31+G(d) basis sets (6-31G basis set augmented with polarization and diffuse functions).[16] The electronic properties of the studied molecular cation were analyzed by means of the natural[17] (NPA) and Mulliken[18] population analyses as well as by the AIM (atoms-in-molecules) approach.[19] To calculate the oscillator strengths, time-dependent (TD) DFT calculations were performed[20] (TD-B3LYP). Two additional stereoisomeric structures not observed in X-ray experiments obtained because of rotations about C6−C8 or C6a−C8 partially double bonds (See Figure 1) were also examined, as well as the rotation profile and energy barrier for such rotations. All quantum mechanical calculations were carried out with the *Gaussian 03*[21] program in the Poznan Supercomputing and Networking Center.

Results and Discussion.

Geometry of MII. A perspective view of the asymmetric part of the unit cell is shown in Figure 1.

The studied molecule constitutes of two imidazopyridine rings (IMP) and a pyridine ring joined together by the bridging sp^2 hybridized carbon atom. The two IMP units substantially differ in their geometric parameters. Bond lengths in these two moieties both measured in X-ray experiment and calculated at the B3LYP/6-31+G(d) level are presented in Table 2, while valence angles are provided as Supporting Information (Table S2).

TABLE 1: Crystal Data and Data Collection and Refinement Parameters for the Investigated Compound

temperature	170 K	130 K
chemical formula	$C_{20}H_{14}N_5O_2Br \times H_2O \times CH_3OH$	
chemical formula weight	486.33	
crystal size (mm^3)	$0.45 \times 0.35 \times 0.20$	
color, habit	green metallic, cube	
crystal system	monoclinic	
space group	$P2_1/c$	
a (Å)	13.824(3)	13.770(3)
b (Å)	11.229(2)	11.219(2)
c (Å)	13.949(3)	13.911(3)
β (°)	107.33(3)	107.47(3)
V ($Å^3$)	2067.0(7)	2049.9(8)
Z	4	
D_x (mg m^{-3})	1.563	1.576
no. of reflections for cell parameters	2814	6257
absorption coefficient (mm^{-1})	2.028	2.045
diffractometer	Kuma KM-4CCD κ-geometry	
monochromator	graphite	
no. of measured reflections	10786	12357
no. of independent reflections	3861	4012
no. of observed reflections	3054	3500
criterion for observed reflections	$I > 2(I)$	
R_{int}	0.0218	0.0209
θ_{max} (°)	25.68	26.06
range of h, k, l	$-16 \le h \le 16$, $-13 \le k \le 7$, $-16 \le l \le 16$	$-16 \le h \le 17$, $-13 \le k \le 8$, $-17 \le l \le 17$
absorption correction	empirical	
T_{min}, T_{max}	0.4807, 0.5732	0.4646, 0.6632
refinement on	F^2	
$R[F^2 > 2\sigma(F^2)]$	0.0261	0.0256
$wR(F^2)$	0.0561	0.0638
S	0.943	1.100
no. of reflections used in refinement	3861	4012
no. of parameters used	360	
H-atom treatment	ΔF_{map}, refined isotropically	
$\Delta\rho_{max}$ (e $Å^{-3}$)	0.265	0.315
$\Delta\rho_{min}$ (e $Å^{-3}$)	−0.241	−0.239

There is an excellent correspondence between geometrical parameters obtained from X-ray crystallography and derived from quantum chemical calculations. The mean unsigned difference between X-ray (170 K) and DFT values amounts to 0.011 Å and 0.53° for bond lengths and valence angles, respectively (not taking into account bonds involving hydrogen atoms). As expected, bond lengths involving H atoms are much shorter in X-ray measurements than in quantum mechanical (QM) calculations. It is mainly due to the fact that from QM calculation one obtains equilibrium distances between nuclei, whereas in X-ray measurements, one gets distances between

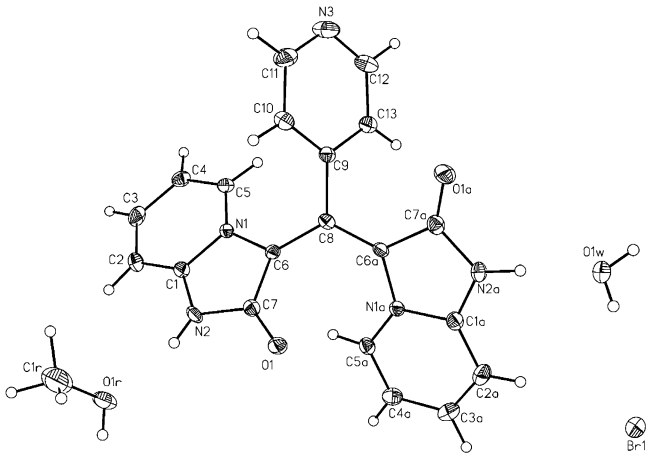

Figure 1. Displacement ellipsoid representation (at 40% probability level) of the asymmetric part of the unit cell and atom numbering scheme.[22] The hydrogen atoms are drawn as spheres of an arbitrary size.

TABLE 2: Bond Lengths in angstroms within the Imidazopyridinium (IMP) Rings Obtained from X-ray Results at 170 K and DFT Calculations, as well as the Calculated Wiberg Bond Indexes (bond orders)

bond lengths	X-ray	DFT	abs |X-ray − DFT|[a]	bond index
O1−C5a	2.855(2)	2.758	0.097	0.026
O1−C7	1.244(2)	1.225	0.019	1.629
O1A−C7a	1.220(2)	1.214	0.006	1.707
N1−C1	1.370(2)	1.379	0.009	1.147
N1A−C1a	1.363(2)	1.378	0.015	1.145
N1−C5	1.378(2)	1.370	0.008	1.163
N1A−C5a	1.371(2)	1.365	0.006	1.170
N1−C6	1.424(2)	1.427	0.003	1.020
N1A−C6a	1.426(2)	1.426	0.000	1.015
N2−C1	1.353(2)	1.358	0.005	1.189
N2A−C1a	1.367(2)	1.358	0.009	1.183
N2−C7	1.391(2)	1.414	0.023	1.021
N2A−C7a	1.386(2)	1.413	0.027	1.021
C1−C2	1.389(3)	1.395	0.006	1.344
C1A−C2a	1.384(3)	1.392	0.008	1.356
C2−C3	1.377(3)	1.386	0.009	1.481
C2A−C3a	1.367(3)	1.388	0.021	1.465
C3−C4	1.397(3)	1.409	0.012	1.343
C3A−C4a	1.400(3)	1.406	0.006	1.356
C4−C5	1.359(3)	1.375	0.016	1.540
C4A−C5a	1.359(3)	1.377	0.018	1.519
C7−C6	1.433(2)	1.452	0.019	1.139
C7A−C6a	1.481(3)	1.478	0.003	1.069
C6−C8	1.419(3)	1.415	0.004	1.301
C6A−C8	1.378(2)	1.394	0.016	1.419
N2−H2N	0.78(2)	1.013	0.233	0.783
N2a−H2Na	0.93(2)	1.013	0.083	0.782
C2−H2	0.91(2)	1.084	0.174	0.908
C2a−H2a	0.89(2)	1.084	0.194	0.908
C3−H3	0.92(2)	1.085	0.165	0.915
C3a−H3a	0.95(2)	1.084	0.134	0.916
C4−H4	0.88(2)	1.084	0.204	0.909
C4a−H4a	0.95(2)	1.084	0.134	0.911
C5−H5	0.93(2)	1.080	0.150	0.911
C5a−H5a	0.89(2)	1.079	0.189	0.917

[a] Mean unsigned difference between X-ray and DFT values = 0.0567 (without H = 0.0112).

electron density maxima. In the case of bonds involving hydrogen atoms, the electron density maxima are significantly shifted from proton centers toward the other atoms involved in bonding.

Two Different Rings: Ionic and meso-Ionic. Comparison between bond lengths of the two different IMP rings coexisting in one molecule shows significant differences. The O1−C7 bond length was measured to be 1.244(2) Å, whereas the O1a−C7a bond was 1.220(2) Å, a striking difference of 0.024(3) Å. For comparison, the O═C bond length in the imidazopyridinium cation has been established by the X-ray method to be 1.199-(3) Å in its chloride salt[23] and 1.202(2) Å in its bromide salt.[24] The carbonyl bond length of 1.244(2) Å is comparable with the values of delocalized C···O double bonds in carboxylate anions or in ureas.[25] In parallel, the C6−C8 bond length is 1.419(3) Å, whereas the corresponding C6a−C8 bond length is 1.378(2) Å, so the former is 0.041(4) Å longer. In the case of the molecule in vacuo, the difference is 0.019 Å. These geometrical parameters clearly indicate that the two formally identical IMP rings, although placed in the very same molecule, are different from one another.

The IMP ring constituting of atoms labeled with "a", whose N1a atom bears a formally positive charge, can be considered the ionic ring. The geometry of this moiety greatly resembles the one established for 2-oxo-2,3-dihydro-1*H*-imidazo[1,2-a]-pyridinium chloride[23] and bromide.[24] The other IMP ring bears

TABLE 3: Point Charges Derived from NPA and Mulliken Population Analyses

atom	Mulliken	NPA	atom	Mulliken	NPA
O1	−0.481	−0.601	H3	0.232	0.276
O1A	−0.440	−0.556	H3A	0.230	0.275
N1	0.188	−0.319	C4	0.001	−0.271
N1A	0.208	−0.314	C4A	−0.447	−0.277
N2	−0.586	−0.609	H4	0.233	0.282
N2A	−0.619	−0.614	H4A	0.225	0.278
H2N	0.468	0.473	C5	−0.023	0.044
H2NA	0.468	0.427	C5A	0.184	0.072
C1	1.232	0.420	H5	0.267	0.273
C1A	1.101	0.434	H5A	0.225	0.261
C2	−0.813	−0.278	C6	−0.814	−0.042
C2A	−0.704	−0.282	C6A	−0.142	0.010
H2	0.232	0.279	C7	0.610	0.640
H2A	0.231	0.279	C7A	0.540	0.609
C3	−0.415	−0.163	C8	0.183	0.025
C3A	−0.424	−0.152			

TABLE 4: Sum of Point Charges Condensed on Atoms Forming Ionic and meso-Ionic IMP Rings Derived from NPA and Mulliken Population Analyses

ring	Mulliken	NPA
meso-ionic	0.331	0.373
ionic	0.636	0.481
difference (I − mI)[a]	0.305	0.108

[a] The positive sign in the calculated difference indicates that electron distribution is altered so that, instead of two rings with the same charge attributed to each of them, some part of the electron cloud is shifted from I to mI ring.

a formally negative charge on O1 and a positive charge on N1; thus, we will further refer to it as the meso-ionic part. The results from QM calculations allowed us to gain insight into the electronic structure of the studied molecule. The NPA and Mulliken derived point charges for ionic and meso-ionic forms are listed in Table 3, while their sums over each of the IMP units are presented in Table 4.

Point charges from Mulliken population analysis exhibit large variations upon going from one atom to its neighbor. In the most extreme example, the point charge on the C1 atom is 1.232 e, while on the neighboring C2 atom, it is −0.813 e. In the case of NPA derived point charges, the amplitude is much more moderate, as C1 bears 0.420 and C2 0.278 e. Figure 2 graphically presents electrostatic potential around molecule. As is clearly visible, the areas of the most negative potential (red) are located close to the pyridine nitrogen atom and carbonylic oxygen atoms, whereas those of the most positive potential (blue) are close to H atoms attached to N2 and N2a. Within the rest of the molecule, there are no strong variations of electrostatic potential. This indicates that large amplitudes of Mulliken point charges result from the physically meaningless, though mathematically simple and elegant, partition of electron densities between neighboring atoms.[26]

Bond Formed between π Aromatic and π^* C═O Orbitals. Data from Table 3 indicate that the carbonyl group is a region where electron distribution differs the most between the two IMP rings. In the case of the ionic IMP ring, point charges indicated by Mulliken analysis are −0.440 e for O and 0.540 e for C, while NPA analysis yields, respectively, −0.556 and 0.609 e. For the meso-ionic IMP ring, point charges from Mulliken analysis are −0.481 and 0.610 e, while NPA produced −0.601 and 0.640 e, for O and C, respectively. The sum of point charges over the IMP rings indicates that the ionic IMP ring gains 0.31 (Mulliken) or 0.11 (NPA) more positive charge. Interestingly, the analysis of natural bonding orbitals (NBO)

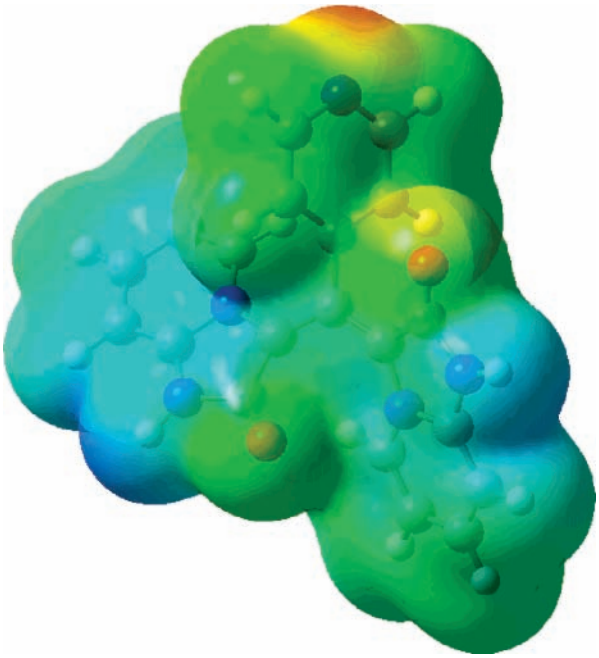

Figure 2. Electrostatic potential mapped on the surface of electron density equal to 0.0004 au is ranging from −0.025 (red) to +0.15 (navy blue).

reveals that the π^* (antibonding) C7═O1 orbital of the meso-ionic ring is partially occupied with 0.41 e, and the calculated Wiberg index for this bond is 1.63. In the case of the ionic IMP ring, a fraction of 0.33 e is attributed to the corresponding π^* (antibonding) C7a═O1a orbital, and the Wiberg index for C7a═O1a is 1.71. This is the reason the two IMP rings are so different.

However, this does not answer a question regarding what happened within the electronic structure of the molecule that resulted in locating one-half of the electron on the C═O π^* orbital. Spin-unrestricted calculations for ground-level singlet state (even when we used triplet optimized wave function as the initial guess) led to the same results. The answer became obvious when we plotted the highest unoccupied molecular orbital (HOMO) of the molecule (see Figure 3). It is clearly visible that the HOMO encompasses the merging π aromatic orbital of the ionic IMP ring and the C═O π^* (antibonding) orbital of meso-ionic IMP ring. The electron isodensity surface plotted around the studied molecule is presented in Figure 4. It shows the electron density bond joining the O1 and C5a atoms. To verify the existence of such a bond, we carried out the AIM analysis to find critical points of the electron density. Indeed, the bond critical point between O1 and C5a was found as presented in Figure 5.

As seen in Figure 5, the bond critical point is placed on the line joining O1 and C5a. The O1−C5a bond is 2.759 Å long, and the critical point is 1.379 Å from the oxygen atom. In the critical point, the electron density is 0.0147 au and the value of the Laplacian of it equals −0.0127 au. For comparison, the values of electron density and its Laplacian in the bond critical point for a planar water dimer (at the same level of theory) are 0.0242 and −0.0212, respectively. The negative value of the Laplacian indicates that the bond between O1 and C5a is primarily of electrostatic character. Indeed, the difference electron density plot (difference between the actual electron density of the molecule and the electron density of the isolated oxygen and carbon atoms) presented in Chart 1 graphically shows that along the line joining O1 and C5a the electron density

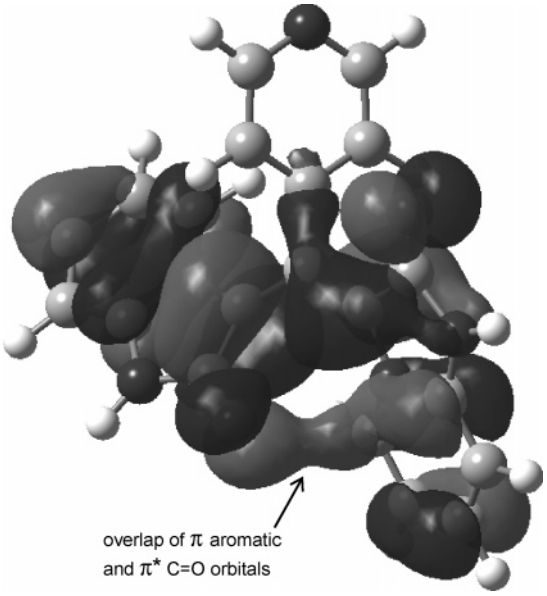

Figure 3. Graphical representation of the HOMO orbital of the molecule.

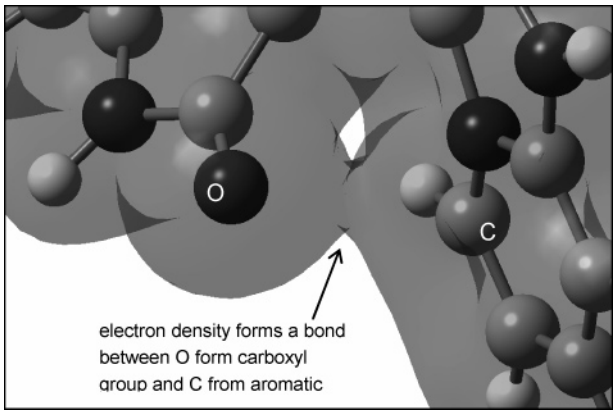

Figure 4. Graphical representation of the electron density around the molecule isodensity surface at 0.015 au. Only the region of interest is shown.

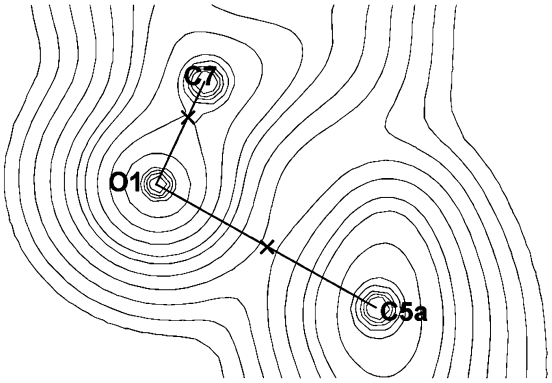

Figure 5. Slice through the molecule with the plane passing through O1, C5A, and C7 showing some aspects of electron density topology: isodensity contour lines, critical bonding points (×), and bonding lines. The critical bonding point between O1 and C5A indicates the presence of a bond between these two atoms.

is shifted toward oxygen, while the C5a carbon atom of the aromatic ring (especially in the region closer to O1) is electron-deficient. It should be mentioned that the formation of this new type of bonding is facilitated by the interaction between the local dipole formed along the C7−O1 bond and the positive charge delocalized in the ionic IMP ring.

CHART 1: Difference Electron Density Plot along O1−C5A Bond[a]

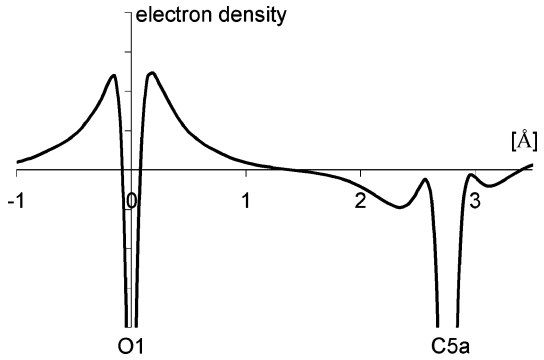

[a] Increase of electron density closer to O1 and decrease close to C5A indicates primarily electrostatic character of the bond.

SCHEME 4: Two Molecules Utilized in Assessment of the Energy of the New Type of Bonding between the Ionic (left) and meso-Ionic (right) IMP Rings.

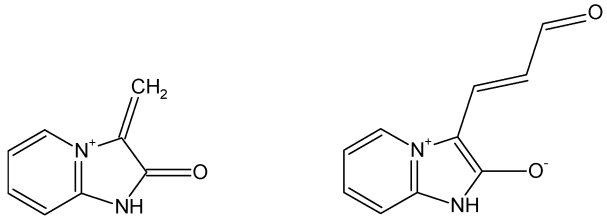

We tried to estimate the energy of such a new type of bonding: π aromatic and π^* C═O. Therefore, we examined energies of the species resembling the interacting IMP rings as shown in Scheme 4.

To assess the energy of the newly identified bond in MII, we carried out B3LYP/6-31+G(d) optimization of the two interacting molecules shown in Scheme 4 with the distance between C (aromatic) and O^- kept constant with the value such as that obtained in the calculations for MII. The energy difference between the separated and interacting molecules equals 3.6 kcal/mol. This value can serve as an estimate of the energy of the intramolecular bond between the π aromatic and π^* C═O observed in MII and is comparable with the energy of weak hydrogen bonds.

Stereoisomeric Structures of MII. Figure 6 presents structures of stereoisomers of MII together with their relative energies and the energies of the transition states connecting these structures.

The cisoidal−cisoidal stereoisomer has energy only 0.1 kcal/mol higher than the cisoidal−transoidal one observed in the crystal structure, but the transoidal−transoidal structure is 8.8 kcal/mol higher in energy. The activation barrier for the rotation around C6−C8 or C6a−C8 bonds is over 20 kcal/mol going from the observed structure to the cisoidal−cisoidal steroisomer and over 21 kcal/mol for the conversion to the transoidal−transoidal stereoisomer. Interestingly, in both the cisoidal−cisoidal and transoidal−transoidal stereoisomers, the two IMP rings present in the molecule are identical with respect to geometrical parameters and electronic structure: a striking difference to the observed cisoidal−transoidal structure. The C═O bond lengths in IMP rings so different in the cisoidal−transoidal stereoisomer (one CO distance of 1.214 Å, the other of 1.225 Å) are of equal value in the transoidal−transoidal structure (both C═O distances of 1.212 Å) and in the cisiodal−cisoidal isomer (both C═O distances of 1.215 Å). This further confirms that in the case of the stereoisomer observed in the

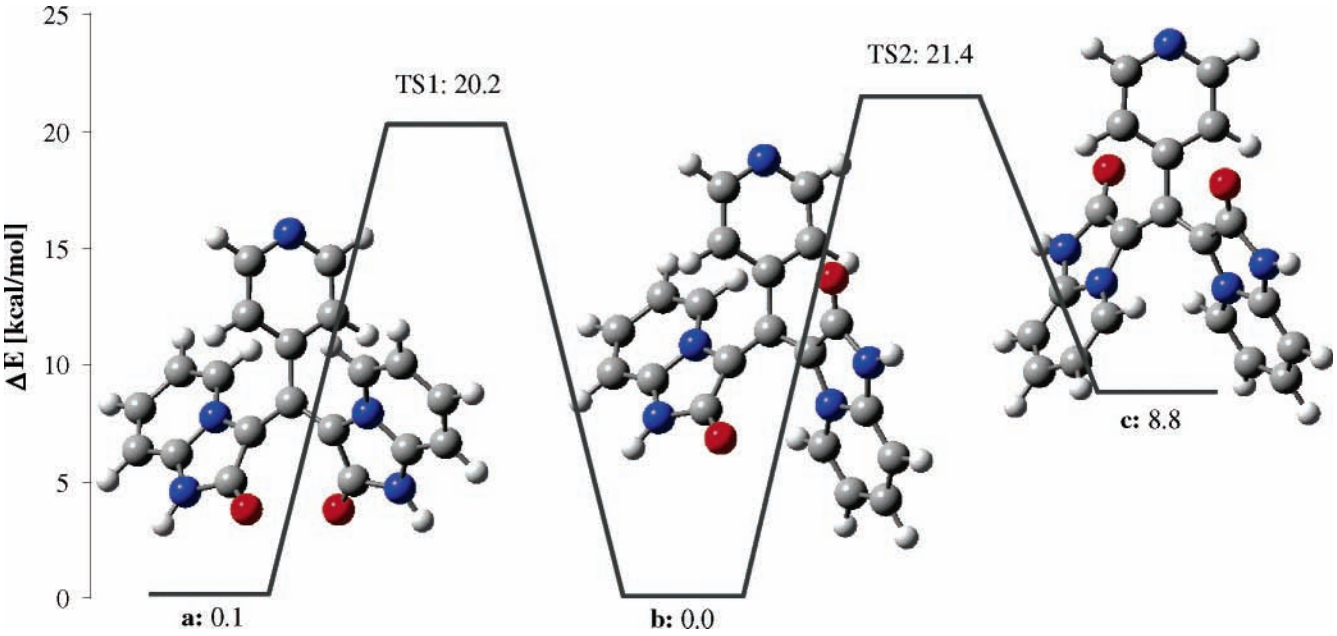

Figure 6. Structures and relative energies of stereoisomers of MII: cisoidal−cisoidal (a), cisoidal−transoidal (b), and transoidal−transoidal (c) obtained by the rotation about partially double C6−C8 or C6a−C8 bonds. Relative energies of transition states shown schematically.

crystal structure and of the lowest energy there exists an intramolecular bond formed as the result of the overlap of π^* C═O antibonding and π aromatic orbitals, hindering the averaging of the two IMP rings in the same molecule.

Despite the Presence of C sp^2 Atoms Only, the Whole MII Structure is Not Planar. Both IMP rings are planar with root-mean-square deviations (rmsd) of 0.030 and 0.034 for the ionic and the meso-ionic form, respectively. For comparison, the rmsd value for the pyridine ring amounts to 0.005. The interplanar angle between the ionic and meso-ionic units is equal to 52.6(0)°, while the angle between each of the two IMP rings and the pyridine ring amounts to 65.4° and 68.6°, respectively. This illustrates that the molecule as a whole is not planar and may be regarded as constituting a rigid frame formed by the bridging, triply substituted carbon atom on which the pyridine and imidazopyridine rings are atached. The sum of the valence angles at this carbon atom is 360°, indicating its sp^2 hybridization. The conformation of the molecule can be described by two sets of torsion angles, each containing the values of torsion angles along the bonds formed by the bridging carbon atom. The torsion angles N1−C6−C8−C9 and C6−C8−C9−C10 amount to 31.1(3)° and 47.0(2)°, while the corresponding values in the ionic part of the molecule are equal to −159.8(2)° and 50.6(2)°, respectively. This illustrates that, with respect to the pyridine substituent, the pyridine nitrogens of the IMP meso-ionic moiety adopt the cisoidal orientation, while those from the ionic moiety adopt the transoidal orientation. Such an arrangement of imidazopyridine moieties creates a left-handed helical arrangement of atoms within the O1−C7═C6−C8═C6a−N1a═C5a−H5a fragment. As mentioned earlier, the quantum chemical calculations indicate the substantial through-space interactions within this fragment that involve the aromatic π and C═O π^* molecular orbitals, (Figures 3 and 4).

It has been known for quite some time already that within the pyridine ring the valence angle at the nitrogen atom is significantly smaller than 120.0° and becomes significantly larger than 120.0° upon protonation. In the investigated compound, this angle amounts to 116.8(2)°, indicating that no protonation takes place at the pyridine ring.

TABLE 5: Oscillator Strengths f_0 and λ_{max} (nm) Recorded for MII in Various Solvents and Calculated in TD-DFT Calculations

medium	f_0	λ_{max}
methanol	0.312	516
pyridine	0.312	535
DMSO	0.370	528
acetonitrile	0.372	515
MP	0.394	536
DMF	0.407	533
in vacuo	0.447	449

Oscillator Strengths. Table 5 presents oscillator strengths and λ_{max} values recorded for MII in various solvents and calculated in TD-DFT calculations. Upon going from one solvent to another, λ_{max} varies from 515 nm recorded in acetonitrile to 535 nm measured in pyridine. Taking into account the facts that the calculations were performed for the isolated molecular cation of MII and that measured λ_{max} strongly depends on the solvent, we find good agreement between the calculated peak at 449 nm and the experimentally measured values. Similarly, the observed oscillator strengths vary from 0.312 in methanol to 0.407 in DMF, so the calculated value of 0.447 is in good agreement with experimental measurements. This indicates that the level of theory employed in calculations is sufficient for obtaining valuable results. The reported data indicate that MII is not a particularly good photoinitiator.

Conclusions

The obtained results indicate the presence of the new type of intramolecular bonding interaction between the aromatic and carbonyl moieties. In the studied molecule, this bond is responsible for structural and electronic differences between the two formally identical IMP rings present in the same molecule. The electronic structure of the studied molecule reveals that the bond in question is formed from sharing some of the electron density between the bonding π aromatic orbital and the antibonding π^* C═O orbital of two different IMP rings. Its character is primarily electrostatic, as the increase of electron density along the bonding line occurs closer to the carbonyl

oxygen atom. Consequently, this oxygen atom gains more negative charge, especially in the area facing the aromatic ring, while the electron density around the aromatic carbon atom in the region facing the carbonyl oxygen atom is decreased, forming there partial positive charge. The energy of this newly detected type of intramolecular bond can be estimated to be 3.5 kcal/mol, a value comparable with weak hydrogen bonds. An analysis of the geometrical parameters and the charge distribution allowed us to propose the MII structure depicted in Scheme 3 as a dominant resonance structure for the investigated molecule.

Acknowledgment. This work was partially financed during the years 2003−2006 by the Polish State Committee for Scientific Research as scientific projects no. 4 T09A 185 25 and 3 T09B 124 26.

Supporting Information Available: Cartesian coordinates of the molecular structure optimized at B3LYP/6-31+G(d) level are collected in Table S1. Valence angles within IMP moieties as obtained from X-ray experiment and DFT calculations are compared in Table S2. This material is available free of charge via the Internet at http://pubs.acs.org.

References and Notes

(1) Baumann, M. E.; Bosshard, H.; Breitenstein, W.; Rist, G.; Winkler, T. *Helv. Chim. Acta* **1984**, *67*, 1897.

(2) Baumann, M. E.; Bosshard, H.; Breitenstein, W.; Rist, G. *Helv. Chim. Acta* **1986**, *69*, 396.

(3) Pyszka, I.; Kucybała, Z.; Pączkowski, J. *J. Polym. Sci., Part A: Polym. Chem.* **2003**, *41*, 3048.

(4) Bonjoch, J.; Fernandez, J-C.; Terricabras, D.; Valls, N. *Tetrahedron* **1997**, *53*, 9407.

(5) Anders, E.; Opitz, A.; Bauer, W. *Synthesis* **1991**, *12*, 1221.

(6) *CrystAlis CCD*, version 1.171; Oxford Diffraction: Oxfordshire, England, 2000.

(7) CCDC contains the supplementary crystallographic data for this paper under the following deposit numbers: CCDC 254878 (170 K) and CCDC 265114 (130 K). These data can be obtained free of charge via www.ccdc.cam.ac.uk/conts/retrieving.html (or from the CCDC, 12 Union Road, Cambridge CB2 1EZ, United Kingdom; fax +44 1223 336033. E-mail: deposit@ccdc.cam.ac.uk).

(8) *CrystAlis RED*, version 1.171; Oxford Diffraction: Oxfordshire, England, 2000.

(9) Sheldrick, G. M. *Acta Crystallogr., Sect. A* **1990**, *46*, 467.

(10) Sheldrick, G. M. *SHELXS-97*; program for the solution of crystal structure; University of Gottingen: Gottingen, Germany, 1997.

(11) Sheldrick, G. M. *SHELXL-97*; program for the refinement of crystal structure; University of Gottingen: Gottingen, Germany, 1997.

(12) *User Manual, Xcalibur Series, Single-Crystal Diffractometers*, version 1.3; Oxford Diffraction: Oxfordshire, England, 2002.

(13) Becke, A. D. *J. Chem. Phys.* **1993**, *98*, 5648.

(14) Parr, R. G.; Yang, W. *Density-functional Theory of Atoms and Molecules*; Oxford University Press: New York, 1989.

(15) Lee, C.; Yang W.; Parr, R. G. *Phys. Rev. B* **1988**, *37*, 785.

(16) (a) Ditchfield, R.; Hehre, W. J.; Pople, J. A. *J. Chem. Phys.* **1971**, *54*, 724. (b) Hehre, W. J.; Ditchfield, R.; Pople, J. A. *J. Chem. Phys.* **1972**, *56*, 2257. (c) Hariharan, P. C.; Pople, J. A. *Mol. Phys.* **1974**, *27*, 209. (d) Gordon, M. S. *Chem. Phys. Lett.* **1980**, *76*, 163. (e) Hariharan, P. C.; Pople, J. A. *Theor. Chim. Acta* **1973**, *28*, 213. (f) Clark, T.; Chandrasekhar, J.; Spitznagel, G. W.; Schleyer, P. v. R. *J. Comput. Chem.* **1983**, *4*, 294. (g) Frisch, M. J.; Pople, J. A.; Binkley, J. S. *J. Chem. Phys.* **1984**, *80*, 3265.

(17) (a) Carpenter, J. E.; Weinhold, F. *THEOCHEM* **1988**, *169*, 4. (b) Foster, J. P.; Weinhold, F. *J. Am. Chem. Soc.* **1980**, *102*, 7211. (c) Reed, A. E.; Weinhold, F. *J. Chem. Phys.* **1983**, *78*, 4066. (d) Reed, A. E.; Weinstock, R. B.; Weinhold, F. *J. Chem. Phys.* **1985**, *83*, 735. (e) Reed, A. E.; Curtiss, L. A.; Weinhold, F. *Chem. Rev.* **1988**, *88*, 899.

(18) Mulliken, R. S. *J. Chem. Phys*. **1955**, *23*, 1833.

(19) *AIM2000*; University of Applied Sciences, Department of Mathematics and Technology; Bielefeld; http://gauss.fh-bielefeld.de/aim2000.

(20) (a) Stratmann, R. E.; Scuseria, G. E.; Frisch, M. J. *J. Chem. Phys.* **1998**, *109*, 8218. (b) Bauernschmitt, R.; Ahlrichs, R. *Chem. Phys. Lett*. **1996**, *256*, 454. (c) Casida, M. E.; Jamorski, C.; Casida, K. C.; Salahub, D. R. *J. Chem. Phys*. **1998**, *108*, 4439.

(21) Frisch, M. J.; Trucks, G. W.; Schlegel, H. B.; Scuseria, G. E.; Robb, M. A.; Cheeseman, J. R.; Montgomery, Jr., J. A.; Vreven, T.; Kudin, K. N.; Burant, J. C.; Millam, J. M.; Iyengar, S. S.; Tomasi, J.; Barone, V.; Mennucci, B.; Cossi, M.; Scalmani, G.; Rega, N.; Petersson, G. A.; Nakatsuji, H.; Hada, M.; Ehara, M.; Toyota, K.; Fukuda, R.; Hasegawa, J.; Ishida, M.; Nakajima, T.; Honda, Y.; Kitao, O.; Nakai, H.; Klene, M.; Li, X.; Knox, J. E.; Hratchian, H. P.; Cross, J. B.; Bakken, V.; Adamo, C.; Jaramillo, J.; Gomperts, R.; Stratmann, R. E.; Yazyev, O.; Austin, A. J.; Cammi, R.; Pomelli, C.; Ochterski, J. W.; Ayala, P. Y.; Morokuma, K.; Voth, G. A.; Salvador, P.; Dannenberg, J. J.; Zakrzewski, V. G.; Dapprich, S.; Daniels, A. D.; Strain, M. C.; Farkas, O.; Malick, D. K.; Rabuck, A. D.; Raghavachari, K.; Foresman, J. B.; Ortiz, J. V.; Cui, Q.; Baboul, A. G.; Clifford, S.; Cioslowski, J.; Stefanov, B. B.; Liu, G.; Liashenko, A.; Piskorz, P.; Komaromi, I.; Martin, R. L.; Fox, D. J.; Keith, T.; Al-Laham, M. A.; Peng, C. Y.; Nanayakkara, A.; Challacombe, M.; Gill, P. M. W.; Johnson, B.; Chen, W.; Wong, M. W.; Gonzalez, C.; Pople, J. A. *Gaussian 03*, Revision B.05; Gaussian, Inc., Wallingford CT, 2004.

(22) *XP*, version 4.2; interactive molecular graphic; Siemens Analytical X-ray Instruments, Inc.: Madison, WI, U.S.A., 1990.

(23) Rybakov, V. B.; Znukov, S. G.; Babaev, E. V.; Mazina, O. S.; Aslanov, L. A. *Kristallografiya* **2000**, *45*, 108.

(24) Plutecka. Unpublished data.

(25) *International Tables for Crystallography*; Wilson, A. J. C., Ed.; Kluwer Academic Publishers: Dordrecht, The Netherlands, 1995; Vol. C.

(26) Hehre, W. J.; Radom, L.; Schleyer P. v. R.; Pople J. A. *Ab Initio Molecular Orbital Theory*; John Wiley & Sons, Inc.: New York, 1986.